Macromolecules

ARTICLE

pubs.acs.org/Macromolecules

Confinement Effects on Chain Entanglement in Free-Standing Polystyrene Ultrathin Films

Jeremy M. Rathfon,[†,‡] Robert W. Cohn,[‡] Alfred J. Crosby,[†] Jonathan P. Rothstein,[†] and Gregory N. Tew[*,†]

[†]Department of Polymer Science and Engineering, University of Massachusetts Amherst, 120 Governors Drive, Amherst, Massachusetts 01003, United States

[‡]ElectroOptics Research Institute and Nanotechnology Center, University of Louisville, Louisville, Kentucky 40292, United States

Supporting Information

ABSTRACT: A study of the confinement effects on chain entanglements in free-standing ultrathin (<100 nm) polymer films is presented. Chain entanglements are probed by determining the lifetime and breakup time scale of a branched network of suspended fibers formed from the annealing of these films. Films of polystyrene (between 50 and 100 nm) cast via flow coating are suspended atop lithographically patterned arrays of pillars. The films are then annealed above the glass transition temperature, where holes are randomly formed. The holes expand exponentially due to capillary forces and impinge upon each other to form a suspended, branched network of fibers. The thinning of fibers as well as the lifetime and breakup of this fiber network is observed via optical microscopy. A model for the viscoelastic-capillary thinning of fibers can be applied to determine a time scale for the breakup of individual samples. The decay of this time scale, below a critical parent film thickness, shows a transition between interchain and self-entanglements when crossing into a confined regime, illustrating a significantly decreased interchain entanglement density and breakdown in the entangled network of the polymer melt. This analysis of confinement effects on chain entanglement extends the understanding of ongoing studies into suspended fiber formation from the melting of free-standing polymer thin films. A better knowledge of chain entanglements in confined systems will make future fabrication of nanoscale suspended fibers, new architectures, and subsequent devices more controlled and accessible.

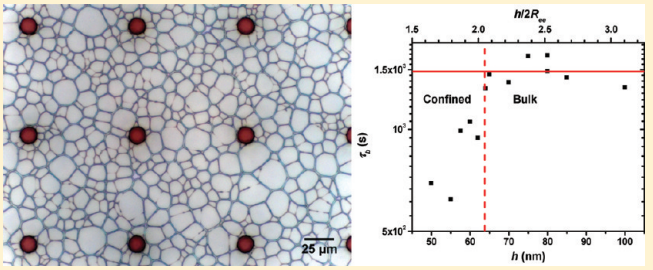

INTRODUCTION

The dynamics of polymer chains in entangled melts has been a major research focus for the past 40 years,[1−9] but few reports directly investigate the entanglement of polymer chains in a confined regime.[10−12] Placing polymer molecules into confined geometries provides a way to probe the effects of confinement on the conformation and mobility of chains and polymer−surface interactions. In the bulk, entangled polymer melts are modeled as ideal Gaussian chains where their random walk motion has a length scale dependent on the molecular weight, M_w, of the polymer.[3] This characteristic length scale of a polymer chain can be expressed by the root-mean-squared end-to-end distance, R_{ee}, where $R_{ee} \sim M_w^{1/2}$. Because of random thermal motions, an ideal chain will explore and occupy a pervaded volume, $V_p \sim R_{ee}^3$. In this volume a polymer chain will have specific interactions with itself and many other chains. Some of these interactions being entanglements or "knots" with other chains, which restrict chain mobility. These entanglements are responsible for many important characteristic polymeric properties including very high melt viscosities, toughness, and elastomeric viscoelasticity.[3,11]

In ultrathin polymer films (less than 100 nm in thickness) the film thickness, h, approaches the natural length scale of a polymer chain (R_{ee}), and as the film thickness decreases, the pervaded volume allowed for a chain's conformation also decreases. Because of increasing confinement, segments from other chains are excluded from a specific chain's pervaded volume, resulting in a reduced interchain entanglement density despite a constant overall entanglement density.[11] In this confined regime, changes in polymer conformation can result in large deviations in phase behavior and dynamics from the bulk.

Confined systems can be explored by studying the formation, evolution, and breakup of suspended fibers formed from the melting of free-standing polystyrene ultrathin films. Hole formation in viscous thin films has been studied in detail in the literature, as in the case of dewetting.[13−20] The nucleation of holes in suspended polymeric films in the melt state has been studied by Rathfon et al.[21] as well as Croll et al.[22] and is found to exhibit a classic free energy barrier relationship, in which hole density, ρ_h, is proportional to the film thickness, h; thus $\rho_h \sim \exp(-h^2)$. The holes expand exponentially under capillary forces and impinge upon each other to form a branched network of suspended fibers. By applying a model for the viscoelastic-capillary thinning and

Received: December 1, 2010
Revised: April 21, 2011
Published: June 08, 2011

dx.doi.org/10.1021/ma1026324 | *Macromolecules* 2011, 44, 5436–5442

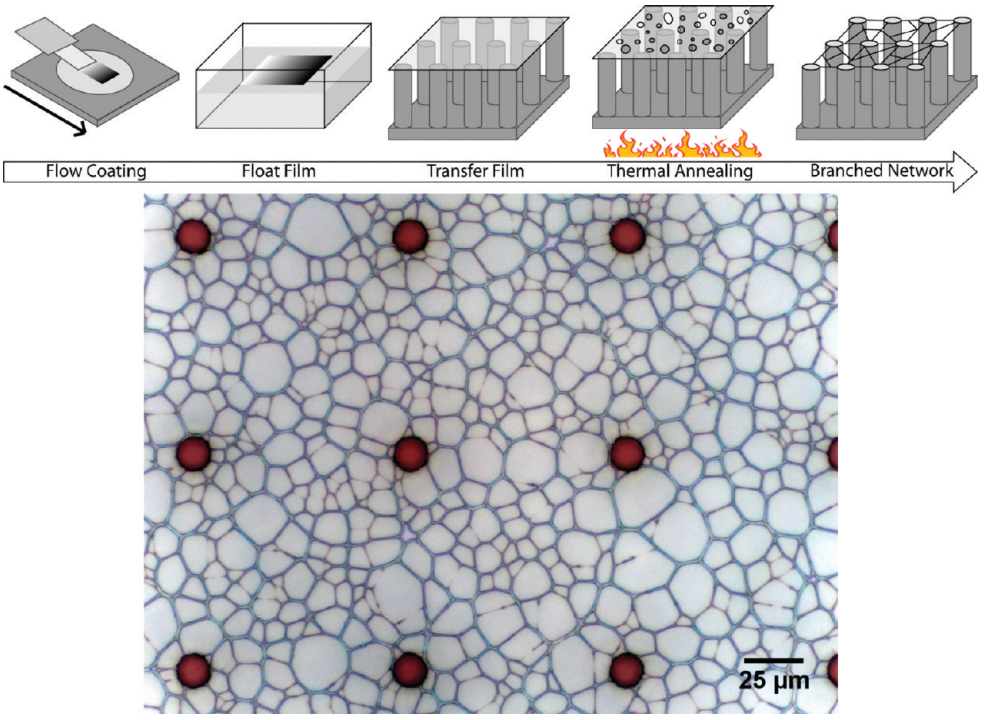

Figure 1. Process for fiber formation via flow coating and thin film melting and a representative image of fiber branching (h = 60 nm, 400 kDa PS). Some fibers have thinned and necked beyond the point of being visible at 50× magnification, which appear as dangling ends. The red uniform circles in the image are the supporting pillars, ∼15 μm in diameter with 75 μm spacing.

breakup of fibers in this network, a characteristic time scale can be derived.

In this study, fiber thinning as well as the branching lifetime and breakup of suspended fibers is investigated via optical microscopy. Ultrathin polystyrene films (h = 50−100 nm), cast via flow coating, are suspended atop lithographically patterned arrays of pillars. The films are then annealed well above the bulk glass transition temperature, T_g, of the polymer, randomly forming holes which expand to form a branched network of fibers. Details of hole expansion[21,23−30] of polymeric thin films have been researched thoroughly in the literature. In this report, the thinning of fiber radius is measured as a function of time and compared for samples of varying molecular weights and thicknesses. The fiber radius evolution is used as a tool to explore rheological properties of these samples. The characteristic time scale for the decay of the branched structures is calculated and compared across the range of film thicknesses. This breakup time scale is dependent on entanglement molecular weight; thus, a transition into a confined regime where interchain entanglements are greatly reduced is shown, evidenced by a corresponding drastic increase in the breakup time scale.

■ RESULTS AND DISCUSSION

Thin Film Preparation. "Flow coating" is a technique, developed by Stafford et al., to fabricate ultrathin polymer films with a gradient thickness in the submicrometer to nanoscale regime, in which a bead of polymer solution is sandwiched between a blade and is drawn across a substrate.[31,32] A schematic of thin film sample preparation for this branching study is given in Figure 1. Gradient thickness polystyrene films, from approximately 50−100 nm in thickness, were cast from 0.75−1.5 wt % solutions in toluene using an acceleration of 6 mm/s^2. Monodisperse polystyrene standard samples were used (PS, M_n = 123, 400, 2000, 6000 kDa, M_w/M_n = 1.08, 1.06, 1.20, 1.22, respectively, Alfa Aesar). After flow coating, film thicknesses were measured across the film's gradient profile via a UV−vis interferometer (Model F20, Filmetrics, Inc.). Films were then floated off the silicon substrate onto clean water (Milli-Q) and subsequently transferred atop a lithographically patterned array of pillars. The pillars have dimensions of 15 μm in diameter and 75 μm spacing. Films were dried and annealed just below the T_g of the polymer film under vacuum for 24 h to remove water and residual solvents.

Fiber Thinning. Ultrathin film samples with varying thicknesses were thermally annealed using an enclosed Linkham LTS350 microscopy thermal stage and imaged via a Zeiss Axio Imager M2m optical microscope at 50× magnification. Film samples were taken from room temperature and heated at 30 °C/min to the annealing temperature, 130 °C for 400 kDa PS, and held while hole formation, subsequent expansion, fiber formation, and branching/fiber breakup occurred. Samples of other molecular weights were annealed at temperatures to match the zero shear rate viscosity, η_0, of this experiment (1.73×10^9 Pa·s), calculated using the empirical WLF equation (116, 161, and 196 °C for 123, 2000, and 6000 kDa, respectively). Previous studies by Rathfon et al. have shown a new approach toward the fabrication of suspended fibers from the melting and breakup of suspended ultrathin, polymer films.[21,33] Upon heating above the T_g of the polymer film, random hole nucleation occurs spontaneously in the suspended films either through a process analogous to spinodal decomposition or from defects such as dust or density inhomogeneities (<0.2 μm).[23,34] Holes observed in this report form spontaneously in the melt in random locations, consistent with literature findings,[23,26,30] and not at the pillar edges. These

dx.doi.org/10.1021/ma1026324 |*Macromolecules* 2011, 44, 5436–5442

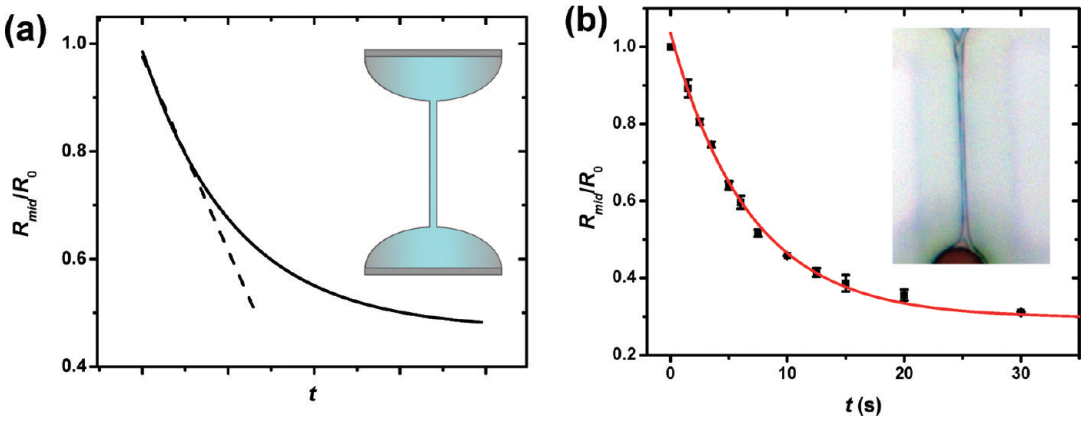

Figure 2. Model for the evolution as a function of time for an elastic fluid filament stretched between two surfaces (a), adapted from McKinley.[36] The dashed line represents the linear response of a Newtonian fluid. A representative plot of the exponential thinning of capillary fibers (b), from a parent film of 100 nm thickness, (400 kDa PS) with an inset of a thinning fiber. Equation 3 was fitted to the data using least-squares-regression.

holes then expand at an exponential rate due to surface tension driven capillary forces competing with viscous dissipation resisting the flow of the polymer.[23−28] As these holes expand, eventually they impinge upon other holes, where the hole edges meet, forming suspended "bridges" or fibers.

The elastocapillary thinning and breakup of slender viscoelastic filaments or fibers has been studied in detail.[35−38] For viscous Newtonian fluids, the time scale for capillary thinning can be expressed as the capillary time $t_{cap} = \eta_0 R/\sigma$, where η_0 is the viscosity, R is the radius, and σ is the surface tension. However, in elastocapillary thinning, fibers neck down and elongate due to capillarity and undergo strong extensional flows which result in large deformations of the polymer molecules leading to large elastic stresses. The strain rate, $\dot{\varepsilon}$, for this capillary thinning, fluid filament can be given as

$$\dot{\varepsilon} = -2\frac{\mathrm{d}\ln(R_{\mathrm{mid}}(t)/R_0)}{\mathrm{d}t} \qquad (1)$$

where R_{mid} is the midfilament radius and R_0 is the initial radius of the filament. For an Oldroyd-B fluid, Entov and Hinch[37] showed that the resulting extension rate is constant and given by $\dot{\varepsilon} = 2/(3\lambda)$, where λ is the Oldroyd relaxation time constant. Anna and McKinley[35,36] later showed that this result is consistent for a number of other viscoelastic constitutive models at moderate strains before the onset of finite extensibility effects (FENE). This includes multimode FENE models as well as the Rouse−Zimm model. However, in each case the Oldroyd relaxation time is replaced by the longest (Zimm) relaxation time, λ_Z. The Rouse−Zimm model predicts this relaxation time to scale with a dependence on chain length with the well-known expression, $\lambda_Z \sim M_w^{3\nu}$, which for a theta solvent ($\nu = {}^1/_2$) is stated $\lambda_Z \sim M_w^{3/2}$.

The total deformation at a given time can be given as the Hencky strain:

$$\varepsilon(t) = \int_0^t \dot{\varepsilon}(t')\,\mathrm{d}t' = 2\ln(R_0/R_{\mathrm{mid}}(t)) \qquad (2)$$

Equation 1 can be rewritten to obtain a prediction for how the radius of a viscoelastic fluid filament will decay with time:

$$\frac{R_{\mathrm{mid}}}{R_0} = \left(\frac{GR_0}{\sigma}\right)^{1/3}\exp(-t/3\lambda_Z) \qquad (3)$$

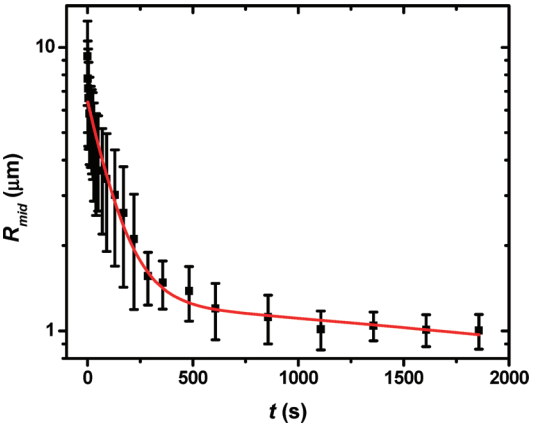

Figure 3. Representative data for the evolution of fiber radius as a function of time, in a semilog plot, exhibiting two regimes of thinning: exponential at early times, as seen by the linear region at $t = 0-300$ s, and transitions to linear at long times, with a different characteristic time scale (h = 65 nm, 400 kDa PS). Note that at $t > 500$ s, a linear region should appear curved in a semilog plot; however, the slope of this region is small and imperceptible on the scale shown. Equation 4 was fitted to the data using least-squares regression.

where G is the elastic modulus, and thus the prefactor in eq 3 can be viewed as the dimensionless elastocapillary number GR_0/σ. This model for the evolution of a viscoelastic fluid filament as a function of time is shown in Figure 2a. The evolution of fiber radius versus time was measured for fibers formed from films with various molecular weights and thicknesses. A representative plot of fiber evolution, showing the exponential decay of fiber radius versus time, for a sample with 100 nm thickness and M_w = 400 kDa, is given in Figure 2b. Fiber radius, R_{mid}, was measured at the midpoint of each fiber from optical microscopy images with an error of ±0.2 μm. Initial fiber radius values measured were typically 30 ± 3 μm. Each data point in the exponential decay curves is from an average of fiber radii from a minimum of five representative fibers. The $R_{mid}(t)/R_0$ curve is fitted via an exponential decay function and accurately depicts the exponential decay of fiber radius for each sample.

The exponential decrease in the fiber radius is well-described with the elastocapillary balance presented in eq 3. However,

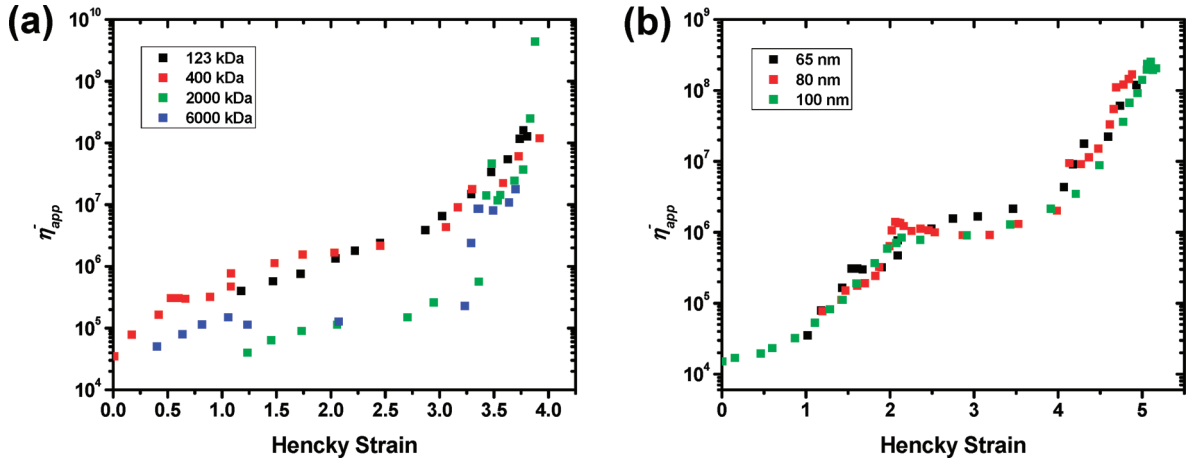

Figure 4. Apparent extensional viscosity, $\bar{\eta}_{app}$, versus Hencky strain, for samples with varying molecular weights (a) and thicknesses (b). Samples with varying M_w had a constant parent film thickness of h = 65 nm, whereas samples with varying thickness had a constant M_w = 400 kDa; pillar spacing was 25 μm.

Entov and Hinch show that radius evolution will approach a linear behavior at late times due to polymer chains becoming fully stretched, no longer being capable of resisting the increasing capillary pressure.[37] At this time, the filament thins similarly to a very viscous Newtonian fluid and approaches a steady-state extensional viscosity, $\bar{\eta}_\infty$. In order to model the two regimes of fiber radius evolution, the following equation is used:

$$\frac{R_{mid}(t)}{R_0} = Ae^{-t/B} - Ct + D \qquad (4)$$

where A, B, C, and D are fitting parameters. The value of B is accordingly related to the longest relaxation time, λ_Z, and σ/C determines the steady-state extensional viscosity, as will be seen in eq 5. Equation 4 is fitted to each sample in order to better model the radius behavior over the two thinning regimes. Figure 3 shows a representative plot of fiber thinning behavior with the model eq 4 applied (see Supporting Information for all curves), clearly showing both the initial exponential decay of fiber diameter then the linear response at long times.

The transient extensional rheology of the PS samples is contained within the fiber radius evolution data and can be reexamined in the form of the transient extensional viscosity or *apparent extensional viscosity*, $\bar{\eta}_{app}$. The forces on the filament form a balance of viscous and viscoelastic stresses with the capillary pressure; thus, by substituting eq 1, $\bar{\eta}_{app}$ is determined to be

$$\bar{\eta}_{app} = \frac{\Delta\tau}{\dot{\varepsilon}} = \frac{\sigma/R_{mid}(t)}{\dot{\varepsilon}(t)} = \frac{-\sigma}{2dR_{mid}/dt} \qquad (5)$$

where $\Delta\tau$ is the tensile stress difference on the filament and $\dot{\varepsilon}$ is the corresponding strain rate.[35,36] Thus, $\bar{\eta}_{app}$ is inversely related to the first derivative of the fiber radius. Experimental data of fiber radius over time were differentiated in order to determine the evolution of apparent extensional viscosity. In Figure 4, $\bar{\eta}_{app}$ is plotted versus Hencky strain for samples with varying molecular weights and parent film thicknesses, thus different initial strain regimes. These initial strain regimes were studied in a previous report where shear viscosity values, for initial hole expansion toward the formation of fibers, were on the order of 10^6 Pa·s with shear strain rates of ~0.5 s^{-1}.[33] The resultant Trouton ratio values for the present study would range between 10^1 and 10^4, consistent with Anna and McKinley's findings for thinning of elastocapillary filaments.[35] It is apparent that a steady-state extensional viscosity plateau was not observed in these fiber thinning experiments. A higher Hencky strain regime could yield these values; however, in the current report, fiber networks typically began to fail before the observation of a steady-state plateau. A recent technique by Arratia et al. shows the acquisition of transient extensional viscosity for polymeric filament thinning in a microfluidic channel, allowing for the attainment of the "elusive" steady-state extensional viscosity.[39,40] The evolution in $\bar{\eta}_{app}$ for samples of varying parent film thicknesses did not change greatly, indicating fibers thinned similarly, for samples of the same M_w, regardless of the differences in their initial strain regimes. This observation is consistent with experimental observation of capillary breakup of polymer solutions and melts and with the predictions of constitutive models like the Oldroyd-B and FENE dumbbell models discussed previously.

Branch Decay. To further probe the effects of confinement on entanglements and the polymer dynamics in free-standing, ultrathin PS films, the evolution of fibers with respect to branching density was investigated. From the expression for the evolution of an elastic fluid capillary fiber (eq 3), the critical time to breakup, t_c, can be expressed as

$$t_c = 3\lambda \ln\left[\frac{4}{3}L^2(GR_0/\sigma)^{4/3}\right] \qquad (6)$$

where λ is the longest relaxation time for the fluid fiber and L is the finite extensibility parameter. Equation 6 is derived from eq 3 as the evolving fiber radius, R_{mid}, approaches zero; however, the finite extensibility of the polymer chain must be considered.[35,36] Thus, t_c gives a time based model for the breakup and decay of the fiber network. Equation 6 shows that the critical time to breakup is dependent upon the longest relaxation time, $t_c \sim \lambda$. Because t_c is proportional to λ, the breakup of fibers in the bulk is dependent upon M_w, which relates directly to the previous statement of $\lambda \sim M_w^{3\nu}$. Thus, there should be a strong correlation between the relaxation time and the effective molecular weight of the chains, dictated by their interchain entanglements, while in a regime with no confinement effects. With confinement, interchain entanglements can be reduced having an influence on the effective molecular weight and thus the relaxation time of the

dx.doi.org/10.1021/ma1026324 |*Macromolecules* 2011, 44, 5436–5442

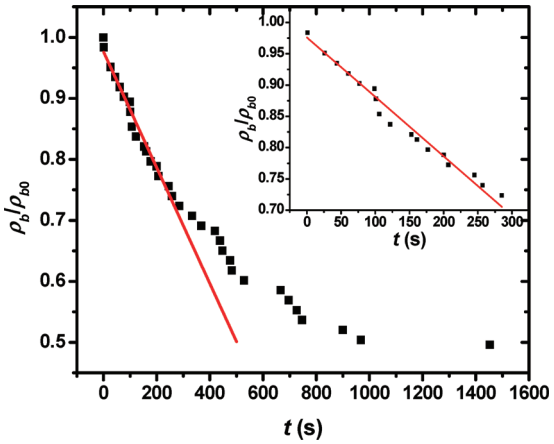

Figure 5. Normalized branch density, ρ_b/ρ_{b0}, as a function of time, t, showing the exponential decay of branching (h = 60 nm, 400 kDa PS) with the initial portion fit with the linear expression, $\rho_b(t)/\rho_{b0} \sim -t/\tau_b$. The inset shows finer detail of the initial linear region of branch density decay.

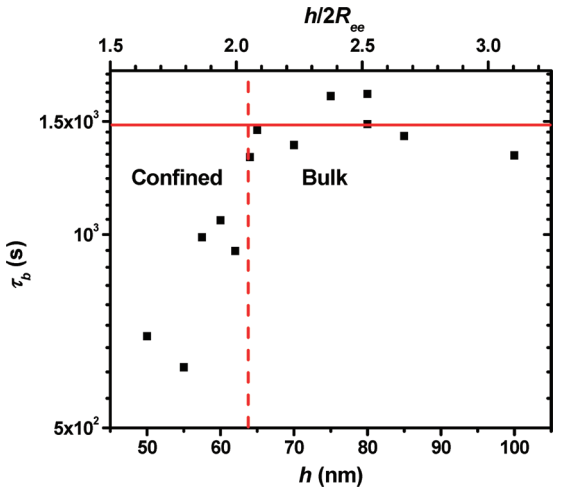

Figure 6. Branching density time scale, τ_b, as a function of film thickness, h, M_w = 400 kDa. The red line is shown to illustrate the deviation from bulk behavior. Thickness is plotted in terms of a dimensionless ratio, $h/2R_{ee}$, along the top axis.

fibers. As the breakup of the fiber network, relaxation time, and the decay of branching in the bulk are all correlated, the following expressions can be stated:

$$\frac{\rho_b(t)}{\rho_{b0}} \sim \exp(-t/\tau_b) \tag{7}$$

$$\tau_b \sim \lambda \sim {M_w}^{3\nu} \tag{8}$$

where $\rho_b(t)$ is the branching density as a function of time, normalized by the initial branching density, ρ_{b0}, and τ_b is the characteristic branching density time scale.

The decay of the branched fiber network is monitored via optical microscopy. From the images, the number of branches and subsequently branching density can be calculated versus time. A representative plot of normalized branch density as a function of time is shown in Figure 5. Branching density falls off linearly in the initial stages of fiber network breakup, and then at long times, breakup slows and the time scale decays. As shown in Figure 5, applying a linear fit to the initial linear portion of the branching data, the characteristic branching density time scale can be acquired, $\rho_b(t)/\rho_{b0} \sim -t/\tau_b$, as the inverse of the tangential slope at t = 0 is equal to the exponential decay constant. A linear fit was chosen to analyze branching density decay due to the time frame of branching experiments at larger thicknesses not completely encompassing the exponential decay of these slower yielding samples. The inset in Figure 5 shows the initial linear region in more detail. Because the branching density time scale is dependent upon t_c (and thus λ and M_w), the slope of the linear portion of the graph should be similar for samples of the same molecular weight, unless the parent film thickness enters the confinement regime. In the confinement regime we would expect a dramatic increase in the magnitude of this slope, thus a decrease in the branching density time scale, indicating less entangled chains, which would contribute to greater yielding and breakup of the fibers.

Confinement Effects on Chain Entanglement. Data for the breakup of fiber networks from parent films with thicknesses varying from 50 to 100 nm were acquired. Branching time scales for this series of films with constant M_w (400 kDa PS) were collected. The plot of linear branching time scales as a function of thickness shows that below a critical film thickness the branching density time scale falls to far less than the expected bulk value (Figure 6). This critical thickness corresponds to the changeover to where the initial film is in a confined regime in which chains have reduced interchain entanglements and thus the film thins, yields, and undergoes breakup more readily in the subsequent flow, indicated by a decreased branching density time scale. In the bulk, τ_b should be directly proportional to the relaxation time of the material, which correspondingly is proportional to the effective M_w. However, once chains have been confined, the branching density time scale and thus the relaxation time deviate. The decrease of the branching density time scale clearly shows its dependence on the effective entanglement molecular weight and therefore the relative entanglement density at a given thickness, $\nu(h)$, thus $\tau_b \sim \nu(h)$. Jones and co-workers illustrate this same confinement regime in their work.[11] They report the same transition to reduced interchain entanglements and increased yielding from films with initial thicknesses below ~60 nm. This difference in yielding behavior between thick and thin films is attributed to a network that is "more loosely entangled".

The amount of confinement of polymer chains in ultrathin films can be expressed as a ratio of film thickness versus the polymer length scale, R_{ee}; thus $h/2R_{ee}$, where $h/2R_{ee}$ = 1, would represent a film with the thickness of one chain's pervaded volume diameter. $2R_{ee}$ was calculated to be ~32 nm for 400 kDa PS according to $R_{ee} = N^{1/2}a$, where N is the number of polymer repeat units and a is the monomer length (approximated to be 2.55 Å).[3] Considering the confined architecture of a thin film, a chain at an air/polymer interface is perturbed and reflected by this boundary such that the pervaded volume of a chain is reduced.[1,11] This perturbation is approximated to be up to 1/2 the bulk pervaded volume. As a chain is perturbed by an interface, the interchain entanglements will be reduced due to the reduction in the allowed pervaded volume. Thus, in a film with two interfaces, such as in a free-standing film, as a film gets thinner, chains will interact with both interfaces and the reduction in pervaded volume and entanglement density becomes more severe. Once a region is entered where films are sufficiently thin,

self-entanglements will dominate and few interchain entanglements will exist, resulting in a drastically reduced network of chains, and thus a more fragile film. Figure 6 shows this reduction in entanglements corresponding to a dimension approximately twice the calculated diameter of a chain in the bulk. Below this dimension perturbation of the pervaded volume of bulk chains is expected to have a significant contribution, as chains would have to begin to pack into a confined regime with the influence of the two air/polymer interfaces. Thus, the entanglement density of the parent film and therefore the time scale for the breakup of the fiber network will be greatly reduced.

The reduced interchain entanglement density seen can be compared to other studies where confinement is shown to affect the chain order, mobility, and dynamics at the surface boundary layer. Baumchen et al. show how interfacial entanglement density affects boundary conditions in polymer flow.[12] Slippage is directly linked to chain entanglements and a reduced interchain entanglement density at the solid−liquid interface is found. The onset of slippage correlates to the critical chain length for entanglements where the slip length dependence on molecular weight corroborates the description by de Gennes for the sliding chain end model.[4] This reduced entanglement density at the boundary layer is similar to our study where a suspended film can be thought of as having two boundaries and thus two surfaces with reduced entanglements. When a film becomes sufficiently thin, these boundary layers can overlap, causing reduced entanglements throughout the film, leading to rapid breakup and a reduced branching density time scale. Bodiguel et al. analyze the dewetting of thin polymer films on a liquid substrate and show a reduced viscosity in thin polymer films.[41] Bodiguel et al. suggest that reduced entanglements in the surface layer allow modes other than reptation, and thus, the viscosity would be reduced in a single surface layer on the order of the coil size. This viscosity reduction, attributed to a reduced interchain entanglement density, is found to depend only on the ratio of film thickness to coil size of the polymer chain. Thus, we would expect a film with two surface layers, such as the free-standing films in this study, to show entanglement reductions near or below a thickness corresponding to two polymer coils as there are two free surfaces. In free-standing films, Dalnoki-Veress et al. showed T_g reduction is dependent on M_w but with no direct link to coil size,[2] contradictory to the findings of Bodiguel et al. where reduced viscosity and thus reductions of entanglements near the surface were directly dependent on coil radius. These discrepancies on coil dependence indicate that shifts in T_g and entanglement reductions are distinct phenomena which operate on length scales affected differently by confinement.

CONCLUSIONS

The thinning of suspended fibers from the melting of free-standing polystyrene thin films was determined to obey the model for the capillary thinning of viscoelastic fluid fibers. The technique of monitoring the evolution of viscoelastic free-standing polymer fibers in the melt can prove to be a useful tool in the study of polymer rheological properties, such as the longest relaxation time of a polymer chain, the apparent extensional viscosity, and the steady-state extensional viscosity. The decay of branching in suspended fiber networks formed by the melting of free-standing polystyrene thin films was determined to be a useful tool in studying the effects of confinement on chain entanglement. Fibers produced from thin films in an initial confined regime, below a critical film thickness, breakup in response to an exponential strain with a characteristic time scale in a manner consistent with a drastic reduction in the interchain entanglement density. The entanglement density was found to decrease in a regime below a corresponding critical parent film thickness, comparable to the dimensions of bulk polymers, $h/2R_{ee} < 2$. This model agrees with previous explorations and experiments with models for the perturbation of the pervaded volume of polymer chains when in contact with interfaces.[1,11] As a film becomes sufficiently thin, interfaces dominate and the proportion of self-entanglements increases and interchain entanglements decrease, resulting in a much less stable network of chains. The presented analysis of confinement effects on chain entanglement extends the understanding of ongoing studies into suspended nanoscale fiber formation from the melting of free-standing polymer thin films.

ASSOCIATED CONTENT

Supporting Information. Fiber radii plots of exponential thinning for all samples; branch density versus time plot for all samples; representative suspended fiber, branch decay movie. This material is available free of charge via the Internet at http://pubs.acs.org.

AUTHOR INFORMATION

Corresponding Author
*E-mail: tew@mail.pse.umass.edu.

ACKNOWLEDGMENT

The authors thank the National Science Foundation's Nanoscale Interdisciplinary Research Team (ECCS 0506941) for their generous support of this work. This work utilized facilities supported in part by the National Science Foundation Materials Research Science and Engineering Center (DMR 0820506) and Center for Hierarchical Manufacturing (CMMI 0531171).

REFERENCES

(1) Brown, H. R.; Russell, T. P. *Macromolecules* **1996**, *29*, 798.
(2) Dalnoki-Veress, K.; Forrest, J. A.; Murray, C.; Gigault, C.; Dutcher, J. R. *Phys. Rev. E* **2001**, *63*, 031801.
(3) de Gennes, P. G. *Scaling Concepts in Polymer Physics*; Cornell University Press: Ithaca, NY, 1979.
(4) de Gennes, P. G. *Eur. Phys. J. E* **2000**, *2*, 201.
(5) Forrest, J. A.; Dalnoki-Veress, K. *Adv. Colloid Interface Sci.* **2001**, *94*, 167.
(6) Graessley, W. W. *Adv. Polym. Sci.* **1974**, *16*, 1.
(7) Keddie, J. L.; Jones, R. A. L.; Cory, R. A. *Europhys. Lett.* **1994**, *27*, 59.
(8) Mattsson, J.; Forrest, J. A.; Borjesson, L. *Phys. Rev. E* **2000**, *62*, 5187.
(9) Roth, C. B.; Dutcher, J. R. *J. Electroanal. Chem.* **2005**, *584*, 13.
(10) Raegen, A.; Chowdhury, M.; Calers, C.; Schmatulla, A.; Steiner, U.; Reiter, G. *Phys. Rev. Lett.* **2010**, *105*, 227801.
(11) Si, L.; Massa, M. V.; Dalnoki-Veress, K.; Brown, H. R.; Jones, R. A. L. *Phys. Rev. Lett.* **2005**, *94*, 127801.
(12) Baumchen, O.; Fetzer, R.; Jacobs, K. *Phys. Rev. Lett.* **2009**, *103*, 247801.
(13) Brochard-Wyart, F.; Debregeas, G.; Fondecave, R.; Martin, P. *Macromolecules* **1997**, *30*, 1211.
(14) Masson, J. L.; Green, P. F. *Phys. Rev. Lett.* **2002**, *88*, 205504.
(15) Reiter, G. *Phys. Rev. Lett.* **1992**, *68*, 75.

(16) Reiter, G. *Langmuir* **1993**, *9*, 1344.
(17) Sharma, A.; Reiter, G. *J. Colloid Interface Sci.* **1996**, *178*, 383.
(18) Vilmin, T.; Raphael, E. *Eur. Phys. J. E* **2006**, *21*, 161.
(19) Reiter, G.; Al Akhrass, S.; Hamieh, M.; Damman, P.; Gabriele, S.; Vilmin, T.; Raphael, E. *Eur. Phys. J.—Spec. Top.* **2009**, *166*, 165.
(20) Seemann, R.; Herminghaus, S.; Jacobs, K. *Phys. Rev. Lett.* **2001**, *86*, 5534.
(21) Rathfon, J. M.; Cohn, R. W.; Crosby, A. J.; Tew, G. N. *Macromolecules* **2011**, *44*, 134.
(22) Croll, A. B.; Dalnoki-Veress, K. *Soft Matter* **2010**, *6*, 5547.
(23) Dalnoki-Veress, K.; Nickel, B. G.; Roth, C.; Dutcher, J. R. *Phys. Rev. E* **1999**, *59*, 2153.
(24) Debregeas, G.; de Gennes, P. G.; Brochard-Wyart, F. *Science* **1998**, *279*, 1704.
(25) Debregeas, G.; Martin, P.; Brochardwyart, F. *Phys. Rev. Lett.* **1995**, *75*, 3886.
(26) Roth, C. B.; Deh, B.; Nickel, B. G.; Dutcher, J. R. *Phys. Rev. E* **2005**, *72*, 021802.
(27) Roth, C. B.; Dutcher, J. R. *Phys. Rev. E* **2005**, *72*, 021803.
(28) Roth, C. B.; Dutcher, J. R. *J. Polym. Sci., Part B: Polym. Phys.* **2006**, *44*, 3011.
(29) Roth, C. B.; Nickel, B. G.; Dutcher, J. R.; Dalnoki-Veress, K. *Rev. Sci. Instrum.* **2003**, *74*, 2796.
(30) Xavier, J. H.; Pu, Y.; Li, C.; Rafailovich, M. H.; Sokolov, J. *Macromolecules* **2004**, *37*, 1470.
(31) Stafford, C. M.; Roskov, K. E.; Epps, T. H.; Fasolka, M. J. *Rev. Sci. Instrum.* **2006**, *77*, 023908.
(32) Meredith, J. C.; Smith, A. P.; Karim, A.; Amis, E. J. *Macromolecules* **2000**, *33*, 9747.
(33) Rathfon, J. M.; Grolman, J. M.; Crosby, A. J.; Tew, G. N. *Macromolecules* **2009**, *42*, 6716.
(34) Brochard-Wyart, F.; Daillant, J. *Can. J. Phys.* **1990**, *68*, 1084.
(35) Anna, S. L.; McKinley, G. H. *J. Rheol.* **2001**, *45*, 115.
(36) McKinley, G. H. *Annu. Rheol. Rev.* **2005**.
(37) Entov, V. M.; Hinch, E. J. *J. Non-Newtonian Fluid Mech.* **1997**, *72*, 31.
(38) Bhardwaj, A.; Miller, E.; Rothstein, J. P. *J. Rheol.* **2007**, *51*, 693.
(39) Arratia, P. E.; Cramer, L. A.; Gollub, J. P.; Durian, D. J. *New J. Phys.* **2009**, *11*, 115006.
(40) Arratia, P. E.; Gollub, J. P.; Durian, D. J. *Phys. Rev. E* **2008**, *77*, 036309.
(41) Bodiguel, H.; Fretigny, C. *Phys. Rev. Lett.* **2006**, *97*, 266105.